Draft version March 18, 2015
Preprint typeset using LaTeX style emulateapj v. 12/16/11

DISCOVERY OF LOW-METALLICITY STARS IN THE CENTRAL PARSEC OF THE MILKY WAY

Tuan Do[1,2,6], Wolfgang Kerzendorf[3,4,7], Nathan Winsor[5], Morten Støstad[3], Mark R. Morris[2], Jessica R. Lu[6], Andrea M. Ghez[2]

Draft version March 18, 2015

ABSTRACT

We present a metallicity analysis of near-infrared K-band (2 μm) spectra of 145 late-type giants within the central 1 pc ($< 20''$) of the Milky Way using adaptive optics with the integral-field spectrograph NIFS on Gemini North. Using spectral template fitting with the MARCS synthetic spectral grid, we find that there is wide range of metallicity, with stars ranging from [Fe/H] < -1.0 to above solar metallicity. This result is in contrast to previous observations, using smaller samples, that show stars at the Galactic center have approximately solar metallicity with only small variations. Our current measurement uncertainties are dominated by systematics in the model, especially at [Fe/H] > 0, where there are stellar lines not represented in the model. However, the conclusion that there are low metallicity stars, as well as large variations in metallicity is robust. We test the method using the IRTF spectral library, which has independent stellar parameter measurements. Some of these low-metallicity stars are consistent with the metallicity of globular clusters, which may be evidence that the nuclear star cluster was formed, at least partially, through globular cluster infall. The high-metallicity stars may have formed closer to the Galactic center or from the disk. In addition our results indicate that it will be important for star formation history analyses using red giants at the Galactic center to consider the effect of varying metallicity.

Subject headings: Galaxy: center — stars: late-type — stars: abundances — techniques: high angular resolution — techniques: spectroscopic

1. INTRODUCTION

The metallicity of stars and stellar populations is an important property that allows us to understand their formation and subsequent evolution. Metallicity can also serve as a signature for separating multiple populations of stars formed at different times. When averaged among many stars, metallicity can be used to trace star formation within and between galaxies.

Chemical abundance measurements of stars in the Milky Way have shown that there is a strong gradient in metallicity (Feltzing & Chiba 2013). The metallicity increases from below solar metallicity in the outskirts of the Milky Way disk to above solar metallicity within the central 5 kpc (Lépine et al. 2011). While the sample of stars in the Milky Way with abundance measurements has increased dramatically with spectroscopic surveys such as APOGEE (Nidever et al. 2014), there abundance measurements of only about a dozen stars in the central 10 pc of the Galaxy (Carr et al. 2000; Ramírez et al. 2000; Cunha et al. 2007,?; Ryde & Schultheis 2014). These measurements are consistent with the Galactic trend, with mean [Fe/H] = 0.14 ± 0.06, and dispersion of 0.16 dex (Cunha et al. 2007).

[1] Dunlap Institute for Astronomy and Astrophysics, University of Toronto, 50 St. George Street, Toronto M5S 3H4, ON, Canada
[2] Physics and Astronomy Department, University of California, Los Angeles, Los Angeles, CA 90095-1547, tdo@astro.ucla.edu
[3] Department of Astronomy and Astrophysics, University of Toronto, 50 St. George Street, Toronto M5S 3H4, ON, Canada
[3] ESO, Garching, Germany
[5] Grenfell Campus - Memorial University of Newfoundland
[6] Dunlap Fellow
[7] ESO Fellow

The metallicity measurements of stars within the central 10 pc of the Galaxy is important, because they form the basis of our interpretation of the formation and properties of the Milk Way nuclear star cluster. This cluster is the most massive (10^7 $M_\odot$) in the Galaxy and provides us with a template for understanding the nuclei of other galaxies (Schödel et al. 2009; Chatzopoulos et al. 2015). The metallicity measurement helps place the cluster in context with the rest of the Galaxy, and serves as a starting assumption when inferring the star formation history and initial mass function (IMF) from the infrared luminosity function (Maness et al. 2007; Pfuhl et al. 2011). It is therefore important to obtain larger spectroscopic samples of stars in this region to obtain robust measurements their physical properties like [Fe/H].

In this study, we combine high angular resolution spectroscopy of red giants with spectral template fitting to directly constrain their effective temperature, gravity, and [Fe/H]. With adaptive optics (AO) spectroscopy, we are able to increase both the depth and the number of stars with measured [Fe/H] in this region by an order of magnitude. This increase in sample size has revealed a number of stars with significantly lower metallicity than have been previously measured in this region. We also discuss the implications of these measurements.

2. OBSERVATIONS

The spectra in this paper were obtained using the Gemini North Near-Infrared Facility Spectrograph (NIFS) with the natural and laser guide star adaptive optics system ALTAIR. The spectra were obtained using the K broad-band filter (1.99 - 2.40 μm) at a spectral resolution of ~ 5000 (GN-2012A-Q-41 and GN-2014A-Q-71, PI: Do). The observations span a projected radius of 8 to 22 arcseconds (0.3 to 0.9 pc) from Sgr A*. More

details about the observations and data reduction were presented by (Støstad et al. 2015). We restrict our analysis here to stars with signal-to-noise ratios (SNR) greater than 10 and $K < 15.5$ in order to better utilize weak spectral lines. We also consider only late-type stars (F-type or later) with temperatures between 2500-7000 K. In total, we analyze 145 stars.

3. SPECTRAL TEMPLATE FITTING

We fit the observed spectra to a MARCS grid of synthetic models to obtain physical parameters (Gustafsson et al. 2008). The MARCS spectral grid[8] spans a range of effective temperature (T_{eff}) between 2500 to 7000 K, surface gravity ($\log g$) between -0.5 and 5.0 dex, and scaled solar metallicity (henceforth described by [Fe/H]) between -4.0 and 1.0 dex. We consider models of solar compositionGrevesse et al. (2007) for this analysis. In order to obtain spectra from intermediate grid parameters, we use a linear interpolation between spectra of neighboring grid points. The MARCS grid (R = 20000) is convolved to R = 5000 for comparison with the NIFS spectra. In addition, we fit a fourth order polynomial to the observed spectrum to normalize its shape. We ignore stellar rotation in our fit because red giants are observed to have rotational velocities below 10 km s^{-1} (Gray 1989), which is not resolvable at the spectral resolution of NIFS. We also limit our fitting range to 2.1 to 2.291 μm to exclude CO lines, which tend to bias our fits (see Section 4.2).

We utilize the Bayesian sampler MultiNest (Feroz et al. 2009) to fit the observed spectra. The fit is done by computing the posterior:

$$P(\theta|D) = \frac{P(D|\theta)P(\theta)}{P(D)} \quad (1)$$

where D is the observed spectrum, and the model parameters $\theta = (T_{eff},\ \log g,\ [\mathrm{Fe/H}], v_z)$, where v_z is the radial velocity. The priors on the model parameters are $P(\theta)$ and $P(D)$ is the evidence, which acts as the normalization. For computational efficiency, we use the log-likelihood in place of the likelihood:

$$\ln P(D|\theta) = -0.5 \sum_{\lambda=\lambda_\circ}^{\lambda_n} ((F_{\lambda,obs} - F_\lambda(\theta))/\epsilon_{\lambda,obs})^2, \quad (2)$$

where $F_{\lambda,obs}$ is the observed spectrum, $F_\lambda(\theta)$ is the model spectrum evaluated with a given set of model parameters, and $\epsilon_{\lambda,obs}$ is the 1 σ uncertainty for each observed flux point. This likelihood assumes that the uncertainty for each flux point is approximately Gaussian. We chose to use MultiNest because the parameter space is often multi-modal, and we find that other techniques like Markov-Chain Monte Carlo are less efficient and often converge at a local maximum instead of the global best-fit solution.

The priors for the model parameters are chosen based on the constraints of the MARCS grid and from stellar evolutionary models for stars that could exist at the Galactic center. The prior on T_{eff} is uniform from 2500 to 8000 K, appropriate for red giants. The prior on [Fe/H] is uniform from -4.0 to 1.0 dex. To determine the limits on $\log g$, we use the PARSEC isochrones (Bressan et al. 2012) for ages between 10^6 to 10^{10} yrs. We then compared the range of $\log g$ with that of the K-band luminosity expected at the Galactic center for these isochrones (Figure 1). Based on these models, we set the priors on $\log g$: -0.5 $< \log g <$ 4.0 for $K < 12$ mag and 2.0 $< \log g <$ 4.5 for $K \geq 12$ mag.

[8] http://marcs.astro.uu.se/index.php

4. CHARACTERIZING UNCERTAINTIES

4.1. *Uncertainty from Interpolation*

While interpolation allows us to produce spectra with arbitrary model parameters, it also increases the uncertainty in the model spectrum. In order to characterize this uncertainty, we remove a grid point, compute an interpolated spectrum at that same point, and then fit the stellar parameters of the interpolated spectrum using the original grid. This represents the maximum deviation due to interpolation, because the interpolated spectra used for our analyses will be, at most, about half the distance from a reference grid point. Repeating this process for the entire grid, we find that $\sigma_{T_{eff}} = 50$ K, $\sigma_{[Fe/H]} = 0.1$, and $\sigma_{\log g} = 0.1$, with no systematic offsets in the fitted parameters. We therefore include the interpolation uncertainty by adding these values in quadrature with the statistical uncertainty for the stellar parameters. This uncertainty is larger than the statistical uncertainties but is small compared to model uncertainties.

4.2. *Fit comparison with standard spectra*

In order to assess possible model uncertainties in the fits, we derive the physical parameters of stars from the SPEX stellar spectral library for comparison to previous measurements (Rayner et al. 2009). While this library has lower spectral resolution (R = 2000) than NIFS (R = 5000), it is the most complete publicly available spectral library in the K-band spanning the range of parameter space of our sample. Importantly, many of the SPEX spectra have been observed previously and have had their stellar parameters measured (tabulated by Cesetti et al. 2013). By comparing to these previous values, we can estimate the range of model uncertainties.

We include constraints on $\log g$ with knowledge of the luminosity of the stars, similar to our analysis of the Galactic center stars. Stars of luminosity class III were limited to $2 < \log g < 4$. Stars with luminosity class I (supergiants) and II were limited to $-0.5 < \log g < 2$. Luminosity class V (main sequence) were limited to $3 < \log g < 5.5$. We also limit the wavelength range of the fit from 2.1 to 2.291 μm, as we find there are significant biases in $\log g$ and [Fe/H] when including CO lines. When compared to the values from Cesetti et al. (2013), the mean and standard deviation of the fit residuals are: $\Delta_{[Fe/H]} = -0.2$, $\sigma_{[Fe/H]} = 0.3$, $\Delta_{\log g} = 1.0$, $\sigma_{\log g} = 0.9$, $\Delta_{T_{eff}} = 50$ K, and $\sigma_{T_{eff}} = 400$. Figure 2 shows the correlation between our fits to that of the literature, and some examples of SPEX spectra compared to our sample with similar [Fe/H]. The offsets from the reference measurements are likely due to systematics in the MARCS model spectra, and the fact that the previous measurements were made by different authors, which can differ by up to 1 dex in [Fe/H] (Cesetti et al. 2013). Observation of these spectral standards with NIFS will

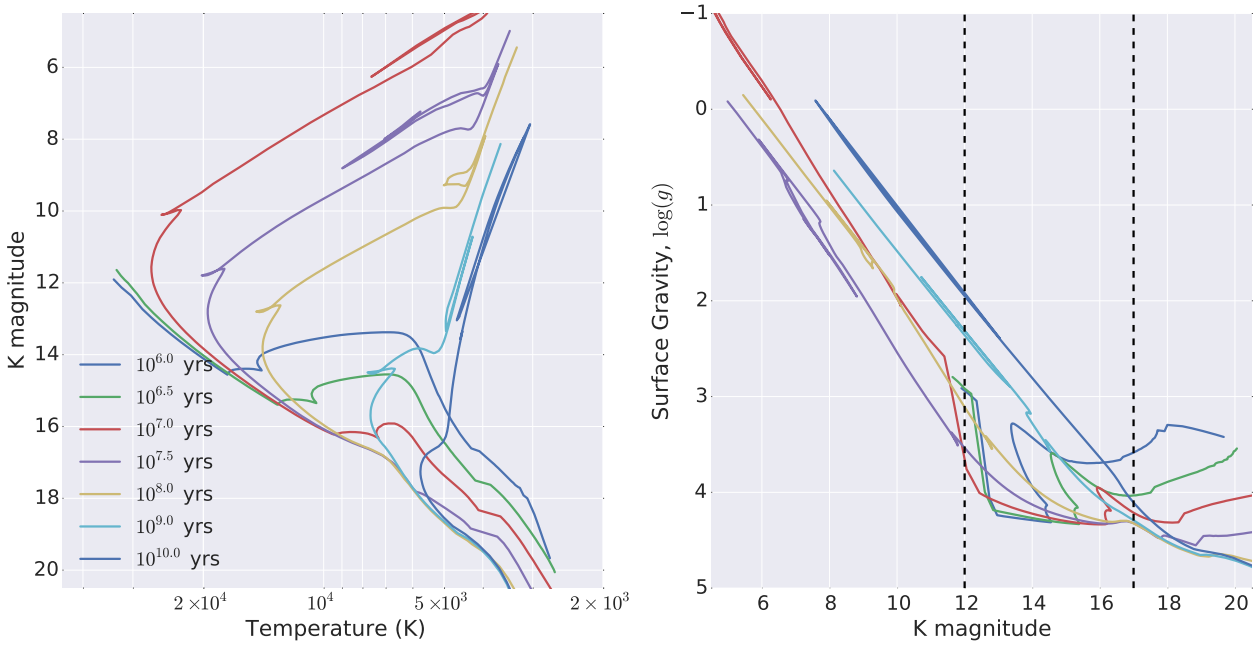

FIG. 1.— **Left:** PARSEC isochrones (Bressan et al. 2012) sampled over the range of observed stellar ages at the Galactic center from the young stars (< 10 Myr) to red giants (1-10 Gyr). **Right:** The surface gravity of stars as a function of K magnitude. We utilize these relationships to limit the range of $\log g$ in the spectral fits. Within the brightness range of most of our measurements (K = 12 - 16 mag), surface gravity varies from $\log g = 4.5$ to $\log g = 2$.

be useful to further quantify the comparison between different abundance measurement techniques. We include these rms values in the uncertainty for our measured parameters by adding them in quadrature with the other uncertainties. These systematic uncertainties dominate over all other sources. The comparison with previous measurements also shows that the $\log g$ values are prone to biases, but the values for [Fe/H] and T_{eff} are consistent to the level of 0.3 dex and 400 K, respectively, which are accurate enough to obtain significant constraints on [Fe/H] and T_{eff} of stars at the Galactic center.

5. RESULTS

For each of the 145 spectra, we fit for the 4 physical parameters: T_{eff}, $\log g$, [Fe/H], and v_z. We report the central value of the probability distribution for each of these parameters marginalized over all other model parameters in Table 1. For most stars in the sample, there are correlations between T_{eff}, $\log g$, and [Fe/H], which emphasizes the necessity to fit them simultaneously. As expected, there is no correlation between v_z and the other 3 parameters. The uncertainties are calculated as described in Section 4.

The fits to the physical parameters reveal the existence of stars with low metallicity at the Galactic center. A glance at the spectra reveals that these stars are unusual; their spectra show low CO, Na, and Ca equivalent widths (e.g. Pfuhl et al. 2011; Do et al. 2013). In Figure 3, we show selected stars with a range of metallicity, from low to super-solar. Figure 3 also shows the best-fit spectra when the metallicity is fixed to [Fe/H] = 0.0. It is clear from the figures that certain lines such as Si I and Fe I are sensitive to [Fe/H]. Other lines, especially H I at 2.1661 μm, are more sensitive to temperature. For example, the star NE1-003 is better fit with a low metallicity of [Fe/H] = -1.27 and $T_{eff} = 4125$ K, compared to one with fixed [Fe/H] = 0.0, and best fit $T_{eff} = 5157$ K (Figure 3). NE1-1 003 lacks the stronger Br γ line at 2.1661 μm that would be required for the $T_{eff} = 5157$ K fit, and contains weak Fe I and Si I lines that are more consistent with low [Fe/H]. While there may be systematic uncertainties in the absolute measurement of [Fe/H], the conclusion that these stars must be low metallicity compared to most of the sample is robust.

Most of the stars have higher than solar metallicity, with about 5% of the stars having [Fe/H] < -0.5. The sample has a mean [Fe/H] = 0.4 with a standard deviation of 0.3 dex. While this suggests that there are many stars with super-solar metallicity at the Galactic center, they are likely subject to greater systematic uncertainties. The MARCS models are unable to reproduce many features in the metal-rich sample. For example, in Figure 3, the star E5-2 001 shows strong features at 2.1898 and 2.2653 μm, which are not present in the MARCS models. This may be due to differences from solar composition or missing atomic and molecular lines in generating the spectra. In order to resolve this discrepancy, it will be necessary to expand the comparison to non-solar composition models. The addition of high spectral resolution observations of some of these sources will also be useful to identify and calibrate the most discriminating lines.

6. DISCUSSION

6.1. *Foreground/background sources and spectroscopic contamination*

Interpretation of the results of this study depends in part on whether the sources belong to the nuclear star cluster, or are foreground or background sources. Some obvious foreground sources can be excluded based on their blue colors, and are not in the

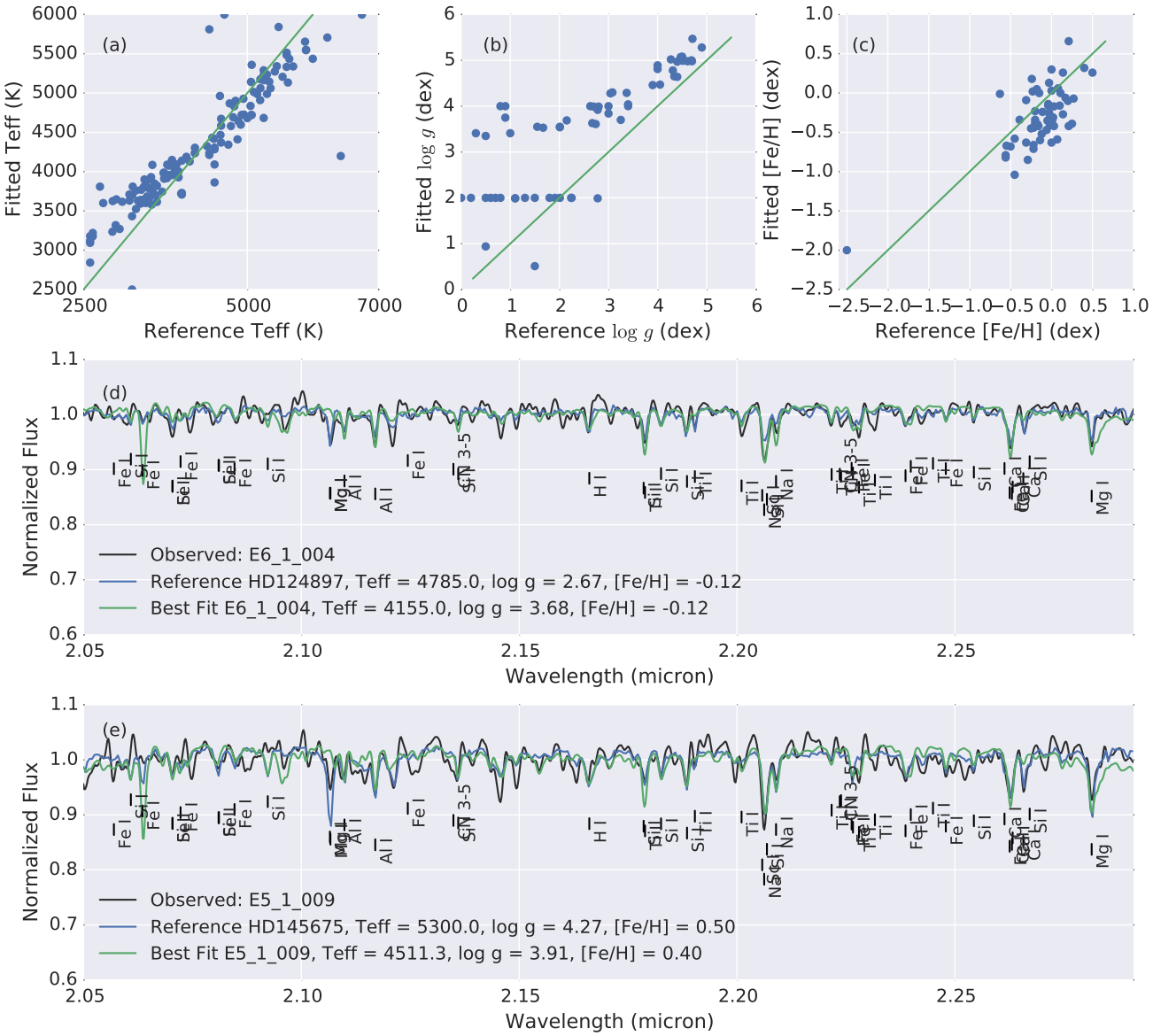

FIG. 2.— Comparison of the best-fit values for the SPEX spectral library to literature values tabulated in Cesetti et al. (2013) for: (a) T_{eff}, (b) $\log g$, (c) [Fe/H]. More stars from SPEX have T_{eff} measurements than $\log g$ or [Fe/H]. Panels (d) and (e) show examples of stars in our sample convolved to the spectral resolution of SPEX (black) compared with a spectrum from the SPEX library with a similar [Fe/H] (blue). The best fit MARCS model (blue) is able to fit most spectral features. Some features, such as Mg I near 2.10 μm and Ca I near 2.27 μm are not well reproduced by the model.

present sample (Støstad et al. 2015). The remaining foreground/background contaminants are likely stars from the inner bulge of the Milky Way. The most recent estimate of the number density of stars in the inner bulge in the near-infrared was made by Clarkson et al. (2012) with their measurement of the proper motion of the Arches star cluster, about 26 pc in projection from the Galactic center. Using their proper motion identification of field stars, we find that the likely number of foreground/background sources is 0.08 stars/arcsec^{-2} with $K < 15.5$. With a coverage of about 99 arcsec^2 in the current survey, we expect about 8 stars to be from the inner bulge. It is possible that some of the low-metallicity stars found in this study belong to the inner bulge, though it is unlikely that this is the case for all of them, as the inner bulge was measured to have on average solar [Fe/H] (Rich et al. 2012; Ryde & Schultheis 2014).

A second source of low-metallicity contamination may be halo interlopers. Using the Besançon Model (Robin et al. 2003), we studied the chance of a contaminant by estimating the number of halo stars expected between 10 – 18 mag in K using an extinction law of $A_V = 3.5$mag/kpc. Within our field of view, the model predicts 0.0004 halo stars, which is negligible.

The presence of a nearby companion would affect the spectra of the stars, biasing the measured stellar parameters. These companions may either be physically close binaries or projected pairs. However, this is unlikely for two reasons: (1) there are very few ($\sim$ 2) early-type stars in the region of this survey (Støstad et al. 2015), so

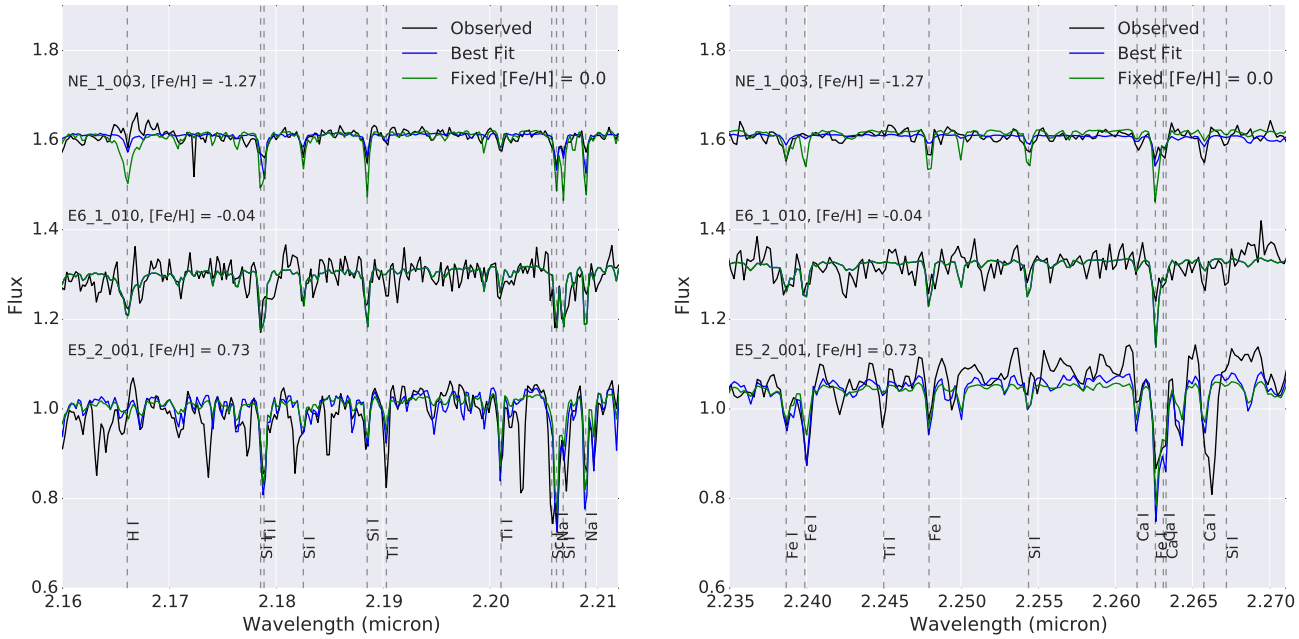

FIG. 3.— Examples of spectra with a range of [Fe/H] along with their best fits (blue) compared to a fit with [Fe/H] fixed to 0.0. The three stars show examples of metal-poor, solar metallicity, and super-solar metallicity stars. These two wavelength regions of K-band were chosen to illustrate the combination of temperature-sensitive lines such as H I compared to metallicity sensitive lines such as Fe I and Si I. The MARCS spectra appear to a good match at solar or below solar metallicities. At high metallicities, the model is unable to reproduce some of the observed lines, likely leading to larger systematic uncertainties in the value of [Fe/H] for these stars.

chance superposition is negligible, (2) physical binaries of a late-type giant and an early-type star are unlikely based on stellar evolution, as the early-type star will have a lifetime of < 100 Myr, while the late-type giant is closer to 1 Gyr in age.

6.2. *Implication for the formation of the nuclear star cluster*

The metallicity of the nuclear star cluster encodes information about its history and initial chemical composition. Until this study no low-metallicity stars have been found there. They may represent stars that were in this region early in the history of the Milky Way, or may have migrated over time to the Galactic center. Another possibility is that these stars arrived through the infall of globular clusters, which we see today with average [Fe/H] similar to the low [Fe/H] stars detected in this study. In fact, one of the prevailing theories for nuclear star cluster formation is that they represent the build up of globular clusters over time (Capuzzo-Dolcetta & Miocchi 2008; Antonini et al. 2012). Measurement of the metallicity of these stars offers a new opportunity to test this theory.

Accounting for the existence of super-solar metallicity stars will also be important to determine the origin of the nuclear star cluster. The origin of these stars may point toward an origin from the Galactic disk, where the metallicity of stars are generally higher. Super-metal rich stars in the solar neighborhood, with [Fe/H] up to 0.6, may be from the inner disk or the Galactic bulge (Trevisan et al. 2011; Bensby et al. 2013; Feltzing & Chiba 2013). In order to determine the origin of these stars in the nuclear star cluster, we will need to identify the systematic uncertainties in the model (Figure 3), and obtain high resolution spectroscopy to measure stellar abundance ratios. Abundance ratios such as [α/Fe], [Ca/Fe], [Si/Fe], etc., can be matched to signatures from other parts of the Galaxy such as the disk, bulge, globular cluster, or local dwarf galaxies.

6.3. *Implication for stellar population analyses*

The detection of the large spread of metallicity of stars at the Galactic center has the potential to change the way we study this region. It may be necessary to revisit the measurements of the star formation history and IMF of the nuclear star cluster (Maness et al. 2007; Pfuhl et al. 2011; Lu et al. 2013). These studies have so far assumed solar metallicity in their models. These analyses require a translation from the luminosity function into a mass function through the use of evolutionary and atmospheric models, which can strongly depend on the metallicity of the stars. In Figure 4, we show a comparison between the K-band luminosity function resulting from 0.5 to 2 $M_\odot$ stars of a cluster with an age of 10^9 yrs with solar metallicity and one with 10 times below solar metallicity. Using the PARSEC evolutionary tracks (Bressan et al. 2012) and a Salpeter IMF, the inferred shape of the K-band luminosity function at the Galactic center is significantly different between the two metallicities.

7. CONCLUSION

We presented stellar parameter estimates using K-band spectra of 145 stars within 1 pc of the center of the Galaxy, and we find a significant spread in metallicity of stars, ranging from 10 times below solar to super-solar metallicities (about 5% of the sample have [Fe/H] below -0.5). This variation in metallicity shows that the Milky Way nuclear star cluster is not composed of a simple stellar population, which previous work has also shown with spectroscopy and luminosity functions (e.g. Maness et al.

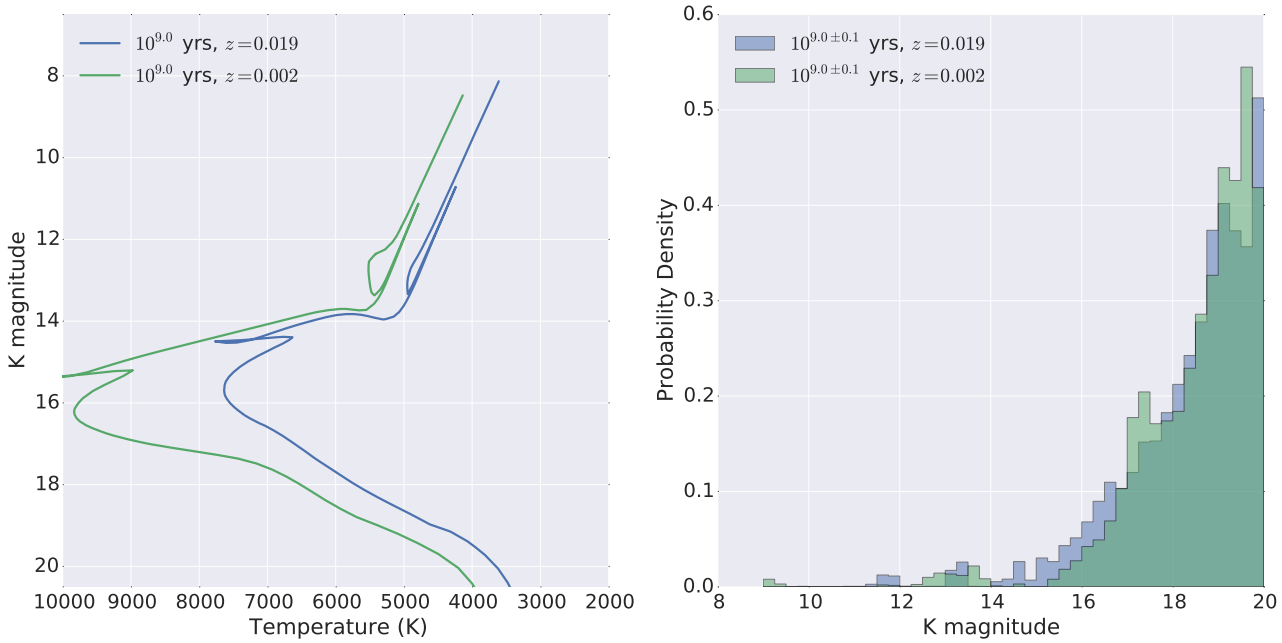

FIG. 4.— **Left:** Evolutionary tracks from the PARSEC model (Bressan et al. 2012) at solar metallicity and a 1/10 solar at 10^9 yrs, showing the difference in temperature and K-band magnitude. The K-band magnitudes are adjusted for the distance to the Galactic center (8 kpc) and the K-band extinction (A_K = 3.0). **Right:** A comparison of the K-band luminosity function of a single-age simple stellar population with a Salpeter IMF at the same metallicities as the plot on the left. This shows that interpretation of the stellar population of the Galactic center can change significantly based on its metallicity.

2007; Chatzopoulos et al. 2015). The low-metallicity stars found in this study are consistent with the range of [Fe/H] observed for globular clusters, which is predicted by the theory that infalling globular clusters contribute to the build up of nuclear star clusters (Capuzzo-Dolcetta & Miocchi 2008; Antonini et al. 2012). The evidence for super-solar metallicity, on the other hand, points towards a significant contribution from stars with origins near the center of the Galaxy (Feltzing & Chiba 2013).

Adding stellar evolutionary models to our fit will allow us to determine the star formation history without the metallicity assumptions that exist in current analysis. In addition, measurement of abundances will allow us to tag the origins (e.g., globular clusters, dwarf galaxies, halo and disk) and build a detailed picture of the assembly of the nuclear cluster in the Milky Way. This can be enhanced further, by also adding kinematic and photometric information to the models.

REFERENCES

Antonini, F., et al. 2012, ApJ, 750, 111
Bensby, T., et al. 2013, A&A, 549, A147
Bressan, A., et al. 2012, MNRAS, 427, 127
Capuzzo-Dolcetta, R., & Miocchi, P. 2008, ApJ, 681, 1136
Carr, J. S., et al. 2000, ApJ, 530, 307
Cesetti, M., et al. 2013, A&A, 549, A129
Chatzopoulos, S., et al. 2015, MNRAS, 447, 952
Clarkson, W. I., et al. 2012, ApJ, 751, 132
Cunha, K., et al. 2007, ApJ, 669, 1011
Do, T., et al. 2013, ApJ, 764, 154
Feltzing, S., & Chiba, M. 2013, New A Rev., 57, 80
Feroz, F., et al. 2009, MNRAS, 398, 1601
Gray, D. F. 1989, ApJ, 347, 1021
Grevesse, N., et al. 2007, Space Sci. Rev., 130, 105
Gustafsson, B., et al. 2008, A&A, 486, 951
Lépine, J. R. D., et al. 2011, MNRAS, 417, 698
Lu, J. R., et al. 2013, ApJ, 764, 155
Maness, H., et al. 2007, ApJ, 669, 1024
Nidever, D. L., et al. 2014, ApJ, 796, 38
Pfuhl, O., et al. 2011, ApJ, 741, 108
Ramírez, S. V., et al. 2000, AJ, 120, 833
Rayner, J. T., et al. 2009, ApJS, 185, 289
Rich, R. M., et al. 2012, ApJ, 746, 59
Robin, A. C., et al. 2003, A&A, 409, 523
Ryde, N., & Schultheis, M. 2014, ArXiv e-prints
Schödel, R., et al. 2009, A&A, 502, 91
Støstad, M., et al. 2015, ApJ, accepted
Trevisan, M., et al. 2011, A&A, 535, A42

TABLE 1
MEASURED PHYSICAL PARAMETERS OF STARS AT THE GALACTIC CENTER

Name	K	SNR	T_{eff} (K)	$\sigma_{T_{eff}}$ [a] (K)	$\log g$	$\sigma_{\log g}$ [a]	[Fe/H]	$\sigma_{[Fe/H]}$ [a]	v_z (km s^{-1})
E5-1 001	12.0	42	3497	413	3.04	0.91	0.96	0.32	-54
E5-1 002	12.6	54	3671	414	2.84	0.91	0.55	0.32	-64
E5-1 003	13.2	44	3597	414	3.09	0.91	0.85	0.32	-58
E5-1 004	13.8	32	3634	416	3.16	0.91	0.90	0.32	-1
E5-1 006	14.7	40	4076	417	3.86	0.91	0.44	0.32	-29
E5-1 007	15.4	41	3754	414	3.18	0.91	0.40	0.32	-57

TABLE 1 — *Continued*

Name	K	SNR	T_{eff} (K)	$\sigma_{T_{eff}}$ [a] (K)	$\log g$	$\sigma_{\log g}$ [a]	[Fe/H]	$\sigma_{[Fe/H]}$ [a]	v_z (km s^{-1})
E5-1 008	15.1	36	3915	418	3.56	0.91	0.43	0.32	-112
E5-1 009	14.8	39	4511	419	3.91	0.91	0.40	0.32	-61
E5-1 010	15.1	31	3724	419	3.24	0.91	0.82	0.32	-102
E5-1 011	15.5	33	4152	417	3.76	0.91	0.64	0.32	1
E5-1 012	15.2	36	4072	420	3.64	0.91	0.63	0.32	112
E5-1 014	15.4	38	4197	421	3.82	0.91	0.27	0.33	-52
E5-1 015	15.7	39	4180	415	3.91	0.91	0.25	0.32	-75
E5-1 016	15.5	42	4145	414	3.89	0.91	0.13	0.32	58
E5-1 017	15.8	26	4274	426	3.36	0.91	-0.17	0.34	-101
E5-1 021	15.5	26	4202	422	3.73	0.91	0.11	0.33	-88
E5-1 042	14.9	35	4161	417	3.82	0.91	0.56	0.32	228
E5-2 001	11.3	60	3519	413	2.92	0.91	0.73	0.32	-63
E5-2 002	13.6	25	3531	415	2.92	0.91	0.97	0.32	147
E5-2 003	14.0	49	3932	419	3.49	0.91	0.02	0.32	-189
E5-2 004	13.9	51	3808	414	3.29	0.91	0.39	0.32	-13
E5-2 005	14.2	38	4328	415	3.85	0.91	0.40	0.32	-29
E5-2 006	14.3	36	4071	418	3.87	0.91	0.45	0.32	157
E5-2 007	14.3	34	3854	415	3.34	0.91	0.60	0.32	-57
E5-2 008	14.6	34	3826	416	3.16	0.91	0.38	0.32	54
E5-2 009	14.9	38	4251	423	3.09	0.91	0.00	0.33	4
E5-2 010	15.1	51	4434	416	3.91	0.91	0.18	0.32	-37
E5-2 011	15.4	41	4613	415	3.94	0.91	0.16	0.32	-13
E5-2 012	15.4	32	4213	418	3.83	0.91	0.09	0.32	294
E5-2 013	15.2	23	4134	426	3.65	0.91	0.53	0.33	45
E5-2 014	15.3	28	3912	424	3.41	0.91	0.66	0.32	-27
E5-2 018	15.4	32	4200	418	3.83	0.91	0.58	0.32	-46
E5-2 019	15.6	37	4131	415	3.69	0.91	0.11	0.32	-21
E6-1 001	12.0	53	3687	413	3.17	0.91	0.60	0.32	84
E6-1 002	12.8	54	3737	414	3.19	0.91	0.47	0.32	-59
E6-1 003	13.3	48	3656	414	3.04	0.91	0.65	0.32	4
E6-1 004	13.3	75	4155	413	3.68	0.91	-0.12	0.32	-61
E6-1 005	13.8	58	3974	414	3.47	0.91	0.33	0.32	-218
E6-1 006	13.8	44	3720	414	3.25	0.91	0.51	0.32	-38
E6-1 008	14.8	38	3986	416	3.68	0.91	0.43	0.32	-4
E6-1 009	14.9	55	4358	413	3.86	0.91	0.41	0.32	-124
E6-1 010	15.4	49	4590	417	3.63	0.91	-0.04	0.32	-105
E6-1 011	14.9	31	4127	418	3.44	0.91	0.42	0.32	-46
E6-1 012	15.4	26	4304	424	3.80	0.91	0.26	0.33	60
E6-1 014	15.4	32	4372	416	3.76	0.91	0.62	0.32	-237
E6-1 020	15.4	20	4039	435	3.56	0.91	0.64	0.33	-30
E6-2 001	13.0	66	3859	414	3.19	0.91	0.43	0.32	46
E6-2 002	13.5	50	3759	413	3.26	0.91	0.39	0.32	-52
E6-2 003	14.0	42	3687	414	3.07	0.91	0.63	0.32	1
E6-2 004	14.0	42	3730	415	3.08	0.91	0.42	0.32	-10
E6-2 005	14.8	36	3836	414	3.30	0.91	0.64	0.32	16
E6-2 006	14.8	41	3898	419	3.47	0.91	0.53	0.32	71
E6-2 007	14.9	33	4692	419	3.75	0.91	0.17	0.32	-47
E6-2 008	15.2	45	4063	415	3.61	0.91	0.24	0.32	-71
E6-2 009	15.1	42	4422	416	3.86	0.91	0.16	0.32	-49
E6-2 010	15.6	31	4227	422	3.18	0.91	-0.31	0.34	-26
E6-2 012	15.2	26	3776	416	3.79	0.91	0.73	0.33	144
E7-1 001	10.8	62	3479	413	2.92	0.91	0.73	0.32	-105
E7-1 002	11.7	56	3662	413	2.96	0.91	0.56	0.32	-70
E7-1 003	12.1	41	3591	414	2.90	0.91	0.76	0.32	35
E7-1 004	12.3	45	3594	414	2.95	0.91	0.72	0.32	-120
E7-1 005	13.4	39	3888	417	3.41	0.91	0.39	0.32	23
E7-1 006	13.5	52	3878	414	3.29	0.91	0.52	0.32	-29
E7-1 007	13.3	64	3479	413	2.83	0.91	0.64	0.32	-118
E7-1 008	14.1	13	3376	420	2.23	0.91	0.97	0.32	116
E7-1 010	14.6	39	3663	416	2.78	0.91	0.41	0.32	-135
E7-1 011	15.3	33	4814	417	0.01	0.91	-1.80	0.35	69
E7-1 022	14.8	38	4218	425	3.63	0.91	0.44	0.32	38
E7-2 001	11.4	51	3524	413	2.85	0.91	0.74	0.32	-189
E7-2 002	14.3	50	3801	414	3.27	0.91	0.39	0.32	-204
E7-2 003	16.0	33	3597	414	3.31	0.91	0.89	0.32	-193
E7-2 004	15.4	34	3616	418	2.96	0.91	0.87	0.32	6
N1-1 001	13.2	44	3644	414	2.99	0.91	0.68	0.32	-47
N1-1 002	13.3	81	4198	413	3.85	0.91	-0.91	0.32	-72
N1-1 003	13.9	46	3844	416	3.36	0.91	0.48	0.32	-128
N1-1 004	14.1	37	3988	417	3.36	0.91	0.36	0.32	-3
N1-1 005	13.6	45	3658	414	3.18	0.91	0.75	0.32	-122
N1-1 006	14.0	34	3668	415	3.20	0.91	0.84	0.32	-173
N1-1 007	14.4	36	3851	415	3.22	0.91	0.61	0.32	79
N1-1 008	14.2	30	3954	416	3.75	0.91	0.41	0.32	109
N1-1 009	14.4	31	3746	416	3.29	0.91	0.47	0.32	-48
N1-1 010	15.2	24	4110	422	3.05	0.91	0.25	0.33	47
N1-1 011	14.9	20	4230	440	2.95	0.91	-1.26	0.37	-238

TABLE 1 — *Continued*

Name	K	SNR	T_{eff} (K)	$\sigma_{T_{eff}}$ [a] (K)	$\log g$	$\sigma_{\log g}$ [a]	[Fe/H]	$\sigma_{[Fe/H]}$ [a]	v_z (km s^{-1})
N1-1 012	14.9	26	4051	421	3.67	0.91	0.35	0.33	8
N1-1 013	14.6	27	3786	419	3.25	0.91	0.78	0.32	-50
N1-1 014	15.1	18	4279	430	3.84	0.91	0.25	0.34	-11
N1-1 015	15.2	28	4126	422	3.57	0.91	0.78	0.33	2
N1-1 016	15.1	19	4324	430	3.73	0.91	0.64	0.33	-229
N1-1 018	15.1	20	3777	434	2.84	0.91	0.48	0.34	-30
N1-1 019	15.7	19	4126	430	3.72	0.91	-0.22	0.35	-77
N1-1 041	14.2	32	3787	419	3.05	0.91	0.68	0.32	98
N1-2 001	13.3	56	3929	415	3.52	0.91	0.40	0.32	57
N1-2 002	13.3	51	3706	413	3.19	0.91	0.67	0.32	53
N1-2 003	13.5	41	3689	413	3.21	0.91	0.65	0.32	60
N1-2 004	13.9	47	3844	413	3.74	0.91	0.36	0.32	137
N1-2 005	14.4	31	4019	421	3.66	0.91	0.64	0.32	135
N1-2 006	14.9	36	4204	420	3.86	0.91	0.39	0.32	30
N1-2 007	14.6	32	3837	416	3.37	0.91	0.54	0.32	-142
N1-2 008	15.0	30	4275	419	3.81	0.91	0.59	0.32	-70
N1-2 009	15.1	34	4774	430	0.29	0.91	-1.85	0.33	21
N1-2 011	15.3	32	3465	415	2.58	0.91	0.62	0.32	-16
N1-2 012	15.5	30	4250	421	3.68	0.91	0.67	0.32	100
N1-2 013	15.3	24	4080	421	3.69	0.91	0.23	0.33	152
N2-1 001	12.1	49	3593	413	3.12	0.91	0.69	0.32	61
N2-1 002	12.1	110	4358	413	3.92	0.91	-1.06	0.32	223
N2-1 003	12.8	43	4260	415	3.82	0.91	-1.20	0.32	31
N2-1 004	13.1	37	3909	415	3.41	0.91	0.18	0.32	48
N2-1 005	13.7	17	3698	422	3.29	0.91	0.29	0.34	-41
N2-1 006	13.6	27	3734	420	3.28	0.91	0.67	0.33	44
N2-1 007	14.2	24	4109	426	3.09	0.91	-0.01	0.33	39
N2-1 008	13.6	18	3513	431	1.14	0.91	0.52	0.36	21
N2-1 009	13.9	19	3939	427	3.74	0.91	0.34	0.33	95
N2-1 012	14.3	23	3568	417	2.92	0.91	0.69	0.33	-79
N2-1 014	15.2	11	3867	454	3.94	0.91	0.07	0.34	-113
N2-2 001	11.5	29	3520	415	3.19	0.91	0.88	0.32	43
N2-2 002	13.1	18	3674	421	3.45	0.91	0.78	0.33	157
N2-2 003	13.5	12	3445	434	2.53	0.91	0.72	0.35	-0
N2-2 004	16.9	15	3450	420	2.56	0.91	0.88	0.33	44
N2-2 005	13.7	11	3861	448	3.29	0.91	0.79	0.35	88
N2-2 006	14.5	13	4135	442	3.50	0.91	0.36	0.35	15
NE1-1 001	10.4	54	3558	414	3.00	0.91	0.80	0.32	55
NE1-1 002	10.7	52	3447	414	2.78	0.91	0.90	0.32	-141
NE1-1 003	11.4	133	4125	413	3.98	0.91	-1.27	0.32	-119
NE1-1 005	12.4	50	3517	413	2.93	0.91	0.89	0.32	-135
NE1-1 007	13.5	39	3710	414	3.21	0.91	0.65	0.32	59
NE1-1 008	13.4	48	3625	415	3.02	0.91	0.81	0.32	-106
NE1-1 009	13.5	52	3683	413	3.27	0.91	0.56	0.32	-43
NE1-1 010	13.9	43	3769	417	3.30	0.91	0.62	0.32	-186
NE1-1 011	14.2	46	3829	414	3.35	0.91	0.56	0.32	34
NE1-1 012	14.5	41	4239	418	3.75	0.91	0.48	0.32	-171
NE1-1 013	14.8	41	3885	422	3.35	0.91	0.33	0.32	-225
NE1-1 014	15.3	38	4241	417	3.92	0.91	0.03	0.32	54
NE1-1 016	15.0	33	3900	416	3.72	0.91	0.68	0.32	-112
NE1-1 017	14.9	25	4103	425	3.57	0.91	0.72	0.33	-94
NE1-1 018	15.1	39	4354	417	3.79	0.91	0.20	0.33	-41
NE1-1 019	16.4	30	4207	424	3.71	0.91	0.23	0.33	44
NE1-1 020	14.9	19	3754	427	3.44	0.91	0.92	0.32	20
NE1-1 021	15.1	28	4084	420	2.63	0.91	0.02	0.33	-73
NE1-1 022	15.1	31	4886	419	3.83	0.91	0.06	0.33	-6
NE1-1 024	15.2	31	4185	425	3.51	0.91	0.68	0.32	-10
NE1-1 025	15.3	52	4224	419	3.66	0.91	0.55	0.32	-39
NE1-1 026	15.5	17	4123	435	3.79	0.91	0.21	0.35	-151
NE1-1 028	15.4	31	4056	419	3.80	0.91	0.35	0.32	-113
NE1-1 030	15.4	25	4803	430	3.90	0.91	0.37	0.33	-8
NE1-1 031	15.3	30	4272	418	3.91	0.91	0.38	0.32	-38

[a] Uncertainties include statistical uncertainties, interpolation uncertainties and systematic uncertainties added in quadrature.